YBULM: 410 | pp. 1–18 (col. fig: NIL) | PROD. TYPE: TEX

ARTICLE IN PRESS

Bulletin of Mathematical Biology (2003) **00**, 1–18
doi:10.1016/j.bulm.2003.10.005

Modeling Activity-Dependent Synapse Restructuring

D. W. VERZI

Department of Mathematics,
San Diego State University-Imperial Valley Campus,
720 Heber Avenue,
Calexico CA 92231,
USA

E-mail: verzi@math.sdsu.edu

The spread of electrical activity in a dendritic tree is shaped, in part, by its morphology. Conversely, experimental evidence is growing that electrical and chemical activity can slowly shape the morphology of the dendrite. In this theoretical study, the dendritic spines are dynamic elements, with biophysical properties that change in response to patterns of electrical activity. Recent experiments and diagrammatic models suggest that activity-dependent processes can regulate structural modifications in dendritic spines as well as their distribution along the dendrite. This study considers how local changes in spine structure (minutes to hours) can influence patterns of electrical activity along the dendrite; and how electrical activity due to synaptic events and excitable membrane dynamics can, over time, influence the morphology of the dendrite.

The model presents a slow subsystem for structural synaptic plasticity associated with long-term potentiation. A perturbation problem evolves naturally when the spine stem shortens, since the ratio of spine stem resistance to input resistance is small. Hence, the difference between the spine head and dendritic potentials become negligible. This paper presents an asymptotic expansion of head potential in terms of dendritic potential. This leads to a reduced model for post-synaptic restructuring that captures the dynamics of the full model in a briefer computation period when the spines are well connected to the dendrite.

1. INTRODUCTION

Dendritic spines are the post-synaptic targets of over 90% of all excitatory synapses in the central nervous system. They are abundant in brain regions associated with learning and memory. Experimental evidence is mounting that the physical structure of a spine and the distribution of spines along the dendrite are modifiable in response to chemical and/or electrical activity (Segev and Rall, 1998; Korkortian and Segal, 1999; Maletic-Savatic *et al*., 1999). For example, in response to activity, spine head volume (and membrane surface area) can increase or decrease; spine necks can change shape from long and slender to short and stubby, and a single synapse on a single spine head can transform into a spine with multiple heads and

0092-8240/03/000001 + 18 $30.00/0

multiple synapses (Geinisman *et al*., 1993; Shepherd, 1996; Harris, 1999a). Consequently, populations of spines on dendritic trees are subject to activity-dependent processes.

Schematic models have been proposed, by experimenters, in order to understand the sequence of events that lead to changes in spine structure and spine count in response to synaptic, electrical, and biochemical activity (Geinisman *et al*., 1993, 1996; Edwards, 1995; Harris, 1999b; Sorra *et al*., 1999). This paper formulates a mathematical description for one of these models (Geinisman *et al*., 1996) and uses it to investigate possible interactions between electrical activity and structural changes in the dendrite. The phenomenological model builds on Wu and Baer's work (Wu and Baer, 1998) for a single spine with an activity-dependent stem conductance. Different in this paper, a continuum of spines is studied over time and space in a system of partial differential equations, extending the cable theory of Baer and Rinzel (Baer and Rinzel, 1991). The spines are stimulated periodically, rather than with a constant current, and active membrane simulations use Hodgkin–Huxley (HH) (Hodgkin and Huxley, 1952) rather than Fitzhugh–Naguma kinetics (FitzHugh, 1969). As a result, the system may be closer to reality, but it is less tractable for analysis.

Simulations explore how activity-dependent changes in spine structure and density may influence patterns of electrical activity, and how electrical activity due to synaptic events and excitable membrane dynamics may, over time, influence spine structure and distribution. The structure of spines is dynamic, changing in time and space in response to changes in local levels of activity, and the local density of spines is a function (over time) of spine structure. The equations governing spine morphology and density comprise a slow subsystem to the cable model. The full system models structural synaptic plasticity associated with long-term potentiation (LTP), based on a schematic proposed by Geinisman (Geinisman *et al*., 1996).

Spine stem resistance has been identified (Rall and Rinzel, 1971) as an important synaptic parameter in that depolarization delivered to the dendrite from passive spines depends critically on the ratio of spine stem resistance to input resistance in the cable (R_{ss}/R_{∞}). Recent observations in the literature indicate that lower values of R_{ss} may be commonplace, rather than the exception (Geinisman *et al*., 1996; Svoboda *et al*., 1996; Boyer *et al*., 1998; Harris, 1999b; Svoboda, 1999; Luscher *et al*., 2000), and occur naturally in the model. A singular perturbation problem evolves when R_{ss}/R_{∞} is small, since this causes the difference between spine head and dendritic potentials to become negligible. An asymptotic expansion of spine head potential leads to a reduced model for synapse restructuring when the spines are well connected to the dendrite.

The model qualitatively captures morphological phenomena observed in recent experiments and is robust for wave propagation dynamics when the spines have active membrane properties. As in recent experiments (Geinisman *et al*., 1993, 1996), a variety of density and structural profiles emerge over time, depending on membrane properties and initial conditions. The paper is organized as follows.

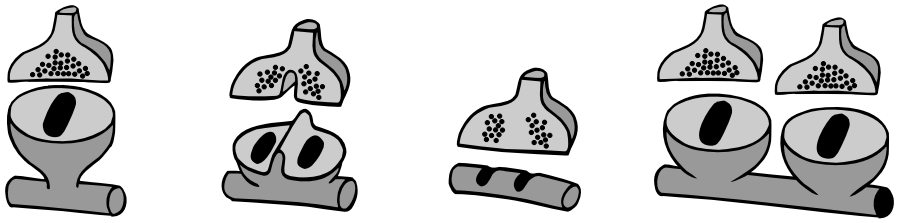

(a) (b) (c) (d)

Figure 1. Activity-dependent synapse restructuring. A single dendritic spine under sustained, high-level activity transitions to two spines after retraction into the dendrite. (a) A spine with a narrow stem that separates the spine head from the parent dendrite. (b) Over time, a spine receiving sustained high levels of activity is partially retracted into the dendrite, and the PSDs are separated. (c) If the activity continues over time, the spine is completed retracted to become two axodendritic synapses, (d) that re-emerge as separate spines [adapted, with permission, from Geinisman *et al*. (1996)].

The model is derived and simulated in Section 2. In Section 3, the reduced model is derived and results are compared to the full model. The last section is the summary and conclusions. A table of parameters, summaries of the formulations, and stability analysis for the cable equation may be found in the appendix.

2. Modeling Activity-Dependent Synapse Restructuring

In Geinisman's model of structural synaptic plasticity (based on electron microscopy), axospinous perforated synapses increase in number shortly after the induction of LTP (Geinisman *et al*., 1993), and are then converted into axodendritic synapses during LTP maintenance (Geinisman *et al*., 1996). He conjectures that in the process of remodeling, the post-synaptic spine may lose its neck to become first partially and then completely retracted into the parent dendrite [see Fig. 4 in Geinisman *et al*. (1996)]. Harris (1999a) comments that Geinisman's observations of LTP maintenance may be an intermediate step toward the creation of two separate synapses, rather than the creation of a single synapse terminating on two post-synaptic densities.

A mathematical description of the above phenomenological model may be based on cable theory (Baer and Rinzel, 1991), which permits the spine density, membrane potentials, and spine stem current to vary continuously in space and time. Since the length and shape of the spine stem is correlated to its resistance and ultimately to stem current flow, it is of interest to explore how the cable model for a continuum of spines along the dendrite may be adapted to simulate Geinisman's diagrammatic model [Fig. 4 in Geinisman *et al*. (1996)].

Fig. 1 depicts the process of activity-dependent synapse restructuring modeled in this paper [adapted, with permission, from Geinisman *et al*. (1996)]. Spines receiving a sustained high level of electrical activity are slowly retracted into the parent

dendrite, to emerge later as two separate dendritic spines. The axospinous synapse in Fig. 1(a) has a spine with a narrow stem that separates it from the dendrite and a single set of PSDs receiving input from the presynaptic axon. In Fig. 1(b), the stem is partially retracted and the PSDs have been split into two sets. [Results from a separate paper Verzi (2000) indicate that merely separating the PSDs, without a corresponding change in spine morphology, will not significantly change a spine's electrical signal.] Fig. 1(c) represents two axodendritic synapses, as the spine stem is completely retracted into the dendrite. If a locally high level of activity continues, they may re-emerge as two separate dendritic spines [Fig. 1(d)].

2.1. ***The cable model.*** The electrical potential $V_d(X,t)$ in a passive dendrite of electrotonic (dimensionless) length $L = l/\lambda$ (l, the physical length), studded with $\overline{n}$ spines per unit length, satisfies the cable equation

$$\tau_m \frac{\partial V_d}{\partial t} = \frac{\partial^2 V_d}{\partial X^2} - V_d + R_\infty \overline{n} I_{ss} \tag{1}$$

(Baer and Rinzel, 1991), where I_{ss} is the spine stem current, τ_m the membrane time constant and $\overline{n}$ the average density of spines at each location $X = x/\lambda$, with λ the length constant. The simulations in this paper assume that both ends of the dendrite are sealed, so that the voltage gradient is always zero at the boundaries, with a resting potential of zero in both the dendritic shaft and spines.

An equation for the membrane potential in each spine head is obtained from a current-balance relation for the capacitive, ionic, synaptic and spine stem currents:

$$C_{sh} \frac{\partial V_{sh}}{\partial t} = -I_{\text{ion}} - I_{\text{syn}} - I_{ss} \tag{2}$$

(Segev and Rall, 1988).

In this paper, the spine stem current is computed as an Ohm's Law voltage drop over the stem resistance

$$I_{ss} = \frac{V_{sh} - V_d}{R_{ss}}, \tag{3}$$

where R_{ss} represents the ratio of specific cytoplasmic resistance to the cross-sectional area, integrated over the length of the stem (Segev and Rall, 1988). If the potential in the spine head is larger than the potential in the dendrite ($V_{sh} > V_d$), then $I_{ss} > 0.0$ and the current flows from spine head to spine base. Conversely, if the potential in the base is larger than the potential in the head ($V_d > V_{sh}$), then $I_{ss} < 0.0$ and current flows from base to head. If $I_{ss} = 0.0$, then no current is passing through the spine stem [see Fig. 1 in Wu and Baer (1998)].

The term I_{ion} represents ionic currents passing through the head membrane and I_{syn} the synaptically applied current. In a simulation involving passive spines $I_{\text{ion}} = V_{sh}/R_{sh}$, but if the spines are considered to have excitable membrane properties,

HH kinetics set to 22 °C (Hodgkin and Huxley, 1952) model voltage-dependent ion channel currents

$$I_{\text{ion}}(V_{sh}, X, t) = \gamma A_{sh}((V_{sh} - V_{Na})\overline{g}_{Na}m^3h + (V_{sh} - V_K)\overline{g}_K n^4 + (V_{sh} - V_L)\overline{g}_L), \tag{4}$$

using increased channel densities (Baer and Rinzel, 1991).

Synapses over a small interval are activated by applying to the spines in that interval

$$I_{\text{syn}}(V_{sh}, X, t) = g_{\text{syn}}(X, t)(V_{sh} - V_{\text{syn}}), \tag{5}$$

where V_{syn} is the synaptic reversal potential and g_{syn} is a brief synaptic conductance generated by the α-function

$$g_{\text{syn}}(X, t) = g_p \frac{t}{t_p} e^{\left(1 - \frac{t}{t_p}\right)}. \tag{6}$$

The continuum description permits simulations involving different distributions of spines and synaptic input patterns. For all simulations in this paper, I_{syn} is applied to the spines at $0.0 \leq X \leq 0.2$.

2.2. ***Activity-dependent spine stem resistance.*** The model now breaks from the formulations of Baer and Rinzel (1991) to view the spine stem current (I_{ss}) as an important measure, over time (minutes to hours), of the electrical activity between the spine head and dendritic base. This paper explores the possibility that this interaction controls slow, local changes in spine structure.

Following Wu and Baer (1998), the model uses stem conductance as a local measure for structural change. They considered a dynamic stem conductance for a single spine in a system of ordinary differential equations as $dG_{ss}(t)/dt = \epsilon I_{ss}$. In the system of partial differential equations presented here, a dynamic stem conductance will vary in time and space as $\partial G_{ss}(X, t)/\partial t = \epsilon I_{ss}$. Since $G_{ss} = 1/R_{ss}$, substituting and rearranging terms, and bounding R_{ss} within a range of established estimates (Segev and Rall, 1988), the rate of change in stem resistance becomes

$$\frac{\partial R_{ss}}{\partial t} = -\epsilon R_{ss}^2 I_{ss} \left(1 - \frac{R_{ss}}{R_{\max}}\right)\left(\frac{R_{ss}}{R_{\min}} - 1\right), \qquad \epsilon \ll 1. \tag{7}$$

Since a significant change in spine structure has been observed over minutes to hours, and individual action potentials (a.p.) are on a time scale of milliseconds (ms), the computation time for a simulation could be of the order of hours. In the simulations that follow, synaptic input is repeated every 10 ms, long enough to allow potentials in the head and dendrite to return to resting values. To identify a value for ϵ that reduces computation time, but preserves the basic dynamics of the system as $\epsilon \to 0$, results were compared during corresponding cycles for different

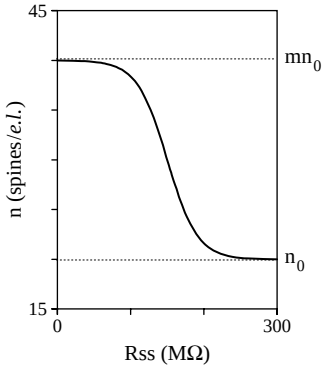

Figure 2. Spine density as a function of stem resistance. Spine density defined by equation (8) is plotted as a function of R_{ss}, setting $m = 2$, $\overline{n}_0 = 20$, $\beta = 30$ and $R_{\text{crit}} = 150$ MΩ. The spine density transitions from n_0 to mn_0 as R_{ss} transitions through R_{crit} from above.

simulations, varying ϵ. For example, results for the time course of a propagating wave of a.p. over 60 cycles of synaptic events using ϵ are superimposed over results of every other cycle from a second simulation, using $\epsilon/2$. As ϵ is successively reduced, the results converge, and ϵ is chosen to be computationally efficient, yet sufficiently small enough to preserve the qualitative structure of the results over longer, real-time evolutions as $\epsilon \to 0$.

2.3. ***Spine density.*** Assume that there is a smooth and relatively rapid transition from one spine to m spines as they become well connected (electrically) to the dendritic shaft, as measured (locally) by the spine stem resistance. The model assumes a value for stem resistance (R_{crit}) that identifies the spines as well connected. The following equation captures the phenomena suggested by Geinisman's model (Geinisman *et al.*, 1996):

$$\overline{n}(X,t) = \overline{n}_0 \left[\frac{m+1}{2} - \frac{m-1}{2} \tanh \frac{\beta(R_{ss}(X,t) - R_{\text{crit}})}{R_\infty} \right], \tag{8}$$

plotted in Fig. 2 for R_{ss} bounded between 0.0 and 300 MΩ, with $R_{\text{crit}} = 150$ MΩ. Here, $\overline{n}_0$ is the initial spine density, and $m\overline{n}_0$ is the maximum spine density. R_∞ is introduced as a scaling factor and β controls the speed of transition.

For R_{ss} low, the spines behave (electrically) like an axodendritic synapse. In equations (7) and (8), current flowing from head to base ($I_{ss} > 0$) slowly causes R_{ss} to decrease. As R_{ss} falls below a critical value (R_{crit}), the spine density may double, triple, etc. (depending on m). Note that in equation (7), R_{ss} increases when $I_{ss} < 0$, allowing for the possibility of reversing the process; Geinisman's diagrammatic model suggests this may be possible (Geinisman *et al.*, 1996). A summary of equations for the full model and a table of parameters may be found in the appendix.

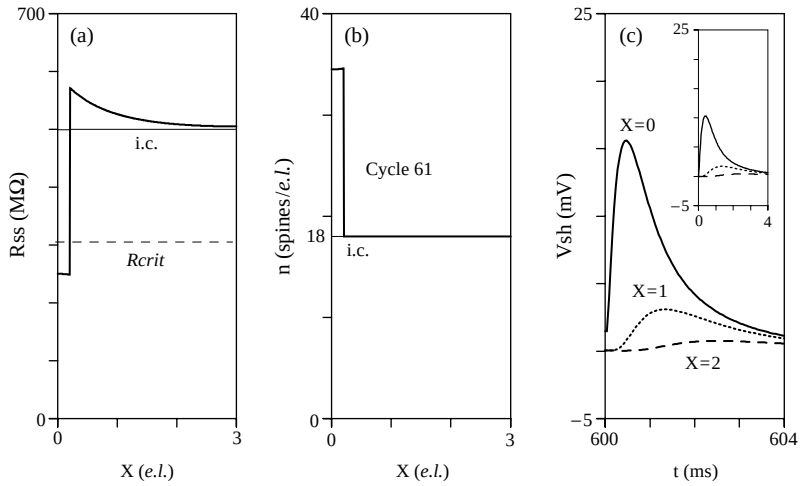

Figure 3. Activity-dependent structural changes mediate passive spine density. A cable of electrotonic length 3 ($\lambda = 179.3\ \mu$m) and diameter 0.36 μm, with both ends sealed, has input resistance $R_\infty = 1233$ MΩ. The dendrite has a uniform distribution of 54 passive spines; spine density (number per λ) is initially $n_0 = 18$. The spine resistance is initially set to a uniform $R_{ss} = 500$ MΩ, above $R_{\text{crit}} = 300$ MΩ. Spines $0 \le X \le 0.2$ are periodically activated every 10 ms with peak conductance 0.74 nS, using I_{syn} given by equation (5). (a) Stem resistance profile superimposed during initial and final cycles of activation. After 30 cycles, $R_{ss} < R_{\text{crit}}$ in the stimulated region, with a slight increase downstream, wherever current is felt. (b) Density profile during initial and final cycles. Spine density has almost doubled in the stimulated region. (c) Time course for head potential during the initial (inset) and final cycles of activation at three locations along the dendrite. Although the number of synapses being activated has almost doubled after 60 cycles, head potential at $X = 0.0$ has increased by only 5 mV due to a corresponding decrease in stem resistance.

2.4. ***Results.*** Of initial interest is how the above interdependent system may affect local structure and density for spines with passive membrane properties. Bounding stem resistance between $R_{\text{min}} = 200$ MΩ and $R_{\text{max}} = 2000$ MΩ, and setting $m = 2$ so that spine density may double as in Geinisman's model (Geinisman *et al.*, 1996), a dendrite of length $L = 3$ is studded with a uniform density of $\overline{n}_0 = 18$ passive spines/$e.l$. The initial structure of these spines is uniformly modeled with stem resistance of $R_{ss} = 500$ MΩ, above $R_{\text{crit}} = 300$ MΩ.

Spines at $0.0 \le X \le 0.2$ are periodically activated with I_{syn} [equations (5) and (6)] every 10 ms, and $I_{\text{ion}} = V_{sh}/R_{sh}$, since the spines are assumed to have passive membrane properties. Fig. 3 graphs the stem resistance profile in (a) and spine density profile in (b) during the initial and 61st cycles of activation (superimposed). A time course for head potential is plotted in (c) during the first 4 ms of the initial (inset) and 61st cycles at three (spatial) locations along the dendrite.

The current is always positive in the stimulated region ($I_{ss} > 0$), causing stem resistance to decrease and the spines to become more electrically connected to the dendrite. Elsewhere, the current flows from dendrite to head ($I_{ss} < 0$), causing

stem resistances to increase and the spines to become more isolated. Compare Fig. 3(a) with 3(b), to observe that after 60 cycles of activation, spine density has nearly doubled in the stimulated region, since local values for R_{ss} have fallen below R_{crit} in response to synaptic activation. An increase of 16 spines/$e.l.$ in the stimulated region of width 0.2 means that approximately four new synapses have been activated there. Elsewhere, $\overline{n}$ remains unchanged and R_{ss} increases wherever current to the extent that current is felt. Compare Fig. 3(c) with its inset to observe that the maximum value for V_{sh} has risen by 5 mV at $X = 0.0$; one might expect more of an increase since the spine density there has almost doubled, but current flows out of these spines more freely since the stem resistance has also decreased!

Also of interest are the effects that this interdependent system may have upon propagation of a.p. when the spines have excitable membrane properties. Fig. 4 graphs results for a second simulation, where 18 spines/$e.l.$ are, again, uniformly located along the dendrite. This time, however, the spines have excitable membrane properties, i.e., I_{ion} is from equation (4). All other parameter and initial values, along with synaptic activation, are as in the previous simulation. The spatial profile for R_{ss} (left) and $\overline{n}$ (center) are shown during selected cycles of activation. A time course for the formation of a propagating wave of a.p. is graphed (right) for three locations along the dendrite, during the same activation cycles as those selected for spatial profiles.

There is no a.p. generated initially for this configuration of density and stem resistance (not shown). However, after 42 cycles, resistance has decreased so that the corresponding spine density at the activation site is just below threshold for a.p. (right) for $R_{ss} = 275$ MΩ. Stem resistance has fallen below R_{crit} (left), causing spine density to increase to $\overline{n} = 33$ in the activated region (center). Outside the stimulated region, stem resistance has increased because these spines are not firing, so that their current source is still from the activated region (i.e., from the dendritic shaft). After 70 cycles, resistance has decreased out to $X = 1.5$ [Fig. 4(b)] in response to generation of local a.p., with a corresponding rise in density. The smallest value for R_{ss} is still in the activated region, as in the passive simulation. Spines with low stem resistance are typically short and broadly based, and offer little resistance to current flow, so that head potential may be well approximated by dendritic potential [c.p. solid and dashed lines in Fig. 4(b) right for $X = 0.0$]. The largest value for R_{ss} over the length of the dendrite is at the point where wave propagation fails. This is also the point where the greatest difference between head and dendritic potentials exists [c.p. solid and dashed lines in Fig. 4(b) right for $X = 1.0$ and 2.0]. After 90 cycles [Fig. 4(c)], stem resistance has fallen below the initial value along the entire dendrite, except immediately downstream of the stimulated region, where base potential dominates due to increased current flowing from newly activated synapses upstream. Wave propagation has decreased R_{ss}, with a corresponding rise in density. A.p. have caused local I_{ss} to be positive and $\partial R_{ss}/\partial t$ negative, on average, for each cycle of activation, allowing $\overline{n}$ to increase and forge a path for impulse propagation.

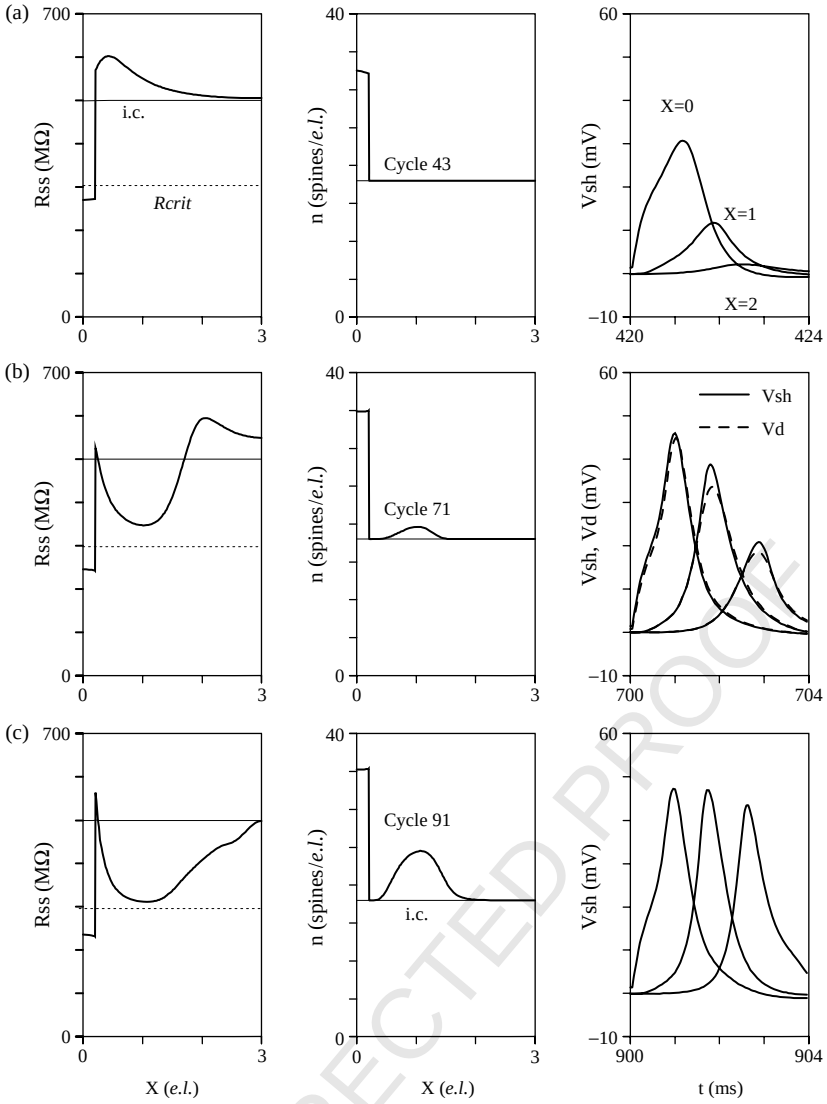

Figure 4. Activity-dependent dendritic structure mediates impulse propagation in spines with excitable membrane properties. A passive cable, with the same geometric and electrical parameters as in Fig. 3, has an initial uniform distribution of 54 excitable spines. Excitable spines have HH membrane in their spine heads; ion channel densities are $\gamma = 2.5$ HH values (HH kinetics for squid at 22 °C). As in Fig. 3, the stem resistance is initially $R_{ss} = 500$ MΩ, above $R_{\text{crit}} = 300$ MΩ, and spines over the input region $0 \leq X \leq 0.2$ are periodically activated every 10 ms with peak conductance 0.74 nS, using equation (5). (a) After 42 cycles, spines in the stimulated region are just below threshold for generating an a.p. (right). R_{ss} has decreased (left) and $\overline{n}$ has increased (center) from synaptic input. (b) After 70 cycles, a.p. propagates to $X = 1.0$, along with corresponding local decreases in R_{ss} and increases in $\overline{n}$. (c) After 90 cycles, a.p. propagates to $X = 2.0$. R_{ss} has fallen below the initial value along the entire length of the dendrite, except immediately adjacent to the activation site. The number of synapses firing a.p. upstream has almost doubled. An increase in density of 18 spines in the stimulated region means that approximately four new synapses have been activated.

3. Modeling Spines that are Well-connected to the Dendrite

The ratio of spine stem resistance to input resistance ($\delta = R_{ss}/R_\infty$) controls how electrically connected the spine is to the dendrite (Segev and Rall, 1988; Shepherd, 1996). When δ is small, the electrical coupling is strong; moreover, as $\delta \to 0$, the governing equations (1)–(3) in the model become singular (see the appendix for a stability analysis of the cable equation). The simulations in Section 2 involving lower values for R_{ss} require reduced time and spatial steps to prevent numerical instabilities, and this dramatically increases computation time.

While experimenters cannot directly measure spine stem resistance, they have inferred values by passing light through the stem and measuring its rate of diffusion. These experiments (Svoboda *et al.*, 1996; Svoboda, 1999) indicate that the lower levels considered in Section 2 may be more realistic than those considered in earlier theoretical studies (Baer and Rinzel, 1971; Segev and Rall, 1988).

Simulations with lower stem resistances involving several hours to days of evolution in dendritic morphology over longer and more complex spine and arbor configurations (Coombes and Bressloff, 2000; Poznanski and Bell, 2000; Vetter *et al.*, 2001; Tsay and Yuste, 2002), will require methods to reduce the computation time. One remedy to this situation is to exploit the perturbation procedure suggested by Baer and Rinzel (1971). As $\delta \to 0$, the difference between spine head and base potentials is negligible, so that one could approximate head potential in terms of base potential, i.e.,

$$V_{sh} = V_d + W_0\delta + W_1\delta^2 + \cdots \tag{9}$$

where $\delta \ll 1$. If $\delta = R_{ss}/R_\infty$, then a first order approximation for the stem current is

$$I_{ss} = \frac{W_0}{R_\infty}. \tag{10}$$

If equations (9) and (10) are substituted into equations (1) and (2) (neglecting terms involving δ), then two first-order formulations for the potential result:

$$\tau_m \frac{\partial V_d}{\partial t} = \frac{\partial^2 V_d}{\partial X^2} - V_d + \overline{n} W_0 \tag{11}$$

$$C_{sh} \frac{\partial V_d}{\partial t} = -I_{\text{ion}}(V_d) - I_{\text{syn}}(V_d) - \frac{W_0}{R_\infty}. \tag{12}$$

Multiply equation (12) by $\overline{n} R_\infty$ and add it to equation (11) to eliminate the last term and recover the HH cable equation (Baer and Rinzel, 1991):

$$(\tau_m + \overline{n} R_\infty C_{sh}) \frac{\partial V_d}{\partial t} = \frac{\partial^2 V_d}{\partial X^2} - V_d - \overline{n} R_\infty (I_{\text{ion}} + I_{\text{syn}}). \tag{13}$$

More specific to this paper, equation (12) may be used to approximate stem current ($I_{ss} = W_0/R_\infty$) as a function of potential, and this value may be used to compute

local changes in structure [I_{ss} in equation (7)]. The functional relation between stem resistance and density in the original system remains unchanged. The new system is stable as $R_{ss}/R_\infty \to 0$, enabling it to capture the dynamics of the full system in $1/25$th of the computation time. A summary of equations for the reduced system may be found in the appendix.

To demonstrate the power of this approximation scheme, results from a different simulation involving active spines are shown in Fig. 5. Bounding stem resistance lower, between $R_{\min} = 40$ and $R_{\max} = 1000$ MΩ, the dendrite is again studded with a uniform density of $\overline{n}_0 = 18$ excitable spines/*e.l.*, but this time the initial stem resistance is uniformly set at $R_{ss} = 300$ MΩ, above $R_{\text{crit}} = 150$ MΩ. All other parameter values, and synaptic and ionic currents are as in Fig. 4.

After 40 cycles, an a.p. is generated in the stimulated region, since R_{ss} has dropped below R_{crit}, causing local spine density to rise above threshold [Fig. 5(a)]. Over time, R_{ss} begins to decrease behind the propagating wave, with a corresponding rise in $\overline{n}$ as $R_{ss} \to R_{\text{crit}}$, out to $X = 1.0$ after 60 cycles [5(b)] and out to $X = 2.0$ after 80 cycles [Fig. 5(c)]. Differences in potential for the two simulations are proportional to δ, with the greatest error occurring when R_{ss} is relatively large. Errors in R_{ss} and $\overline{n}$ depend on the error for V_d and accumulate over time. The greatest difference in R_{ss} for each cycle occurs just in front of the propagating wave, where δ has been large over the greatest period of time.

It is interesting to note that the magnitude of the propagating wave of a.p. [Fig. 5(c)] is greatest in the center of the dendrite. Spine density upstream is larger, but stem resistance is smaller, allowing current to flow out of the spines more freely. On the other hand, spines downstream have higher stem resistances to impede current flow, but the density has not yet increased there.

For the purpose of graphing, incremental steps are the same for both simulations. However, when the reduced model is run again with larger incremental steps, results are qualitatively similar, and can be obtained in $1/25$th of the computational time, since the reduced model is stable as $R_{ss} \to 0$.

4. Summary and Conclusions

This paper considers one way to model the interdependence of activity and morphology in the dendrite by studying specifically observed phenomena. Spine structure responds to changes in activity levels and density approaches a maximum value in areas of sustained activity, as measured by the spine stem current. However, the formulation does not allow density to fall below its initial condition. An interesting question for future work is how to formulate a dynamic spine density that can range from 0.0 to a maximum value, and to consider simulations where the activation site is randomly selected in each cycle.

The model qualitatively captures observed phenomena and predicts a general increase in spine density, as well as a higher percentage of spines more electrically

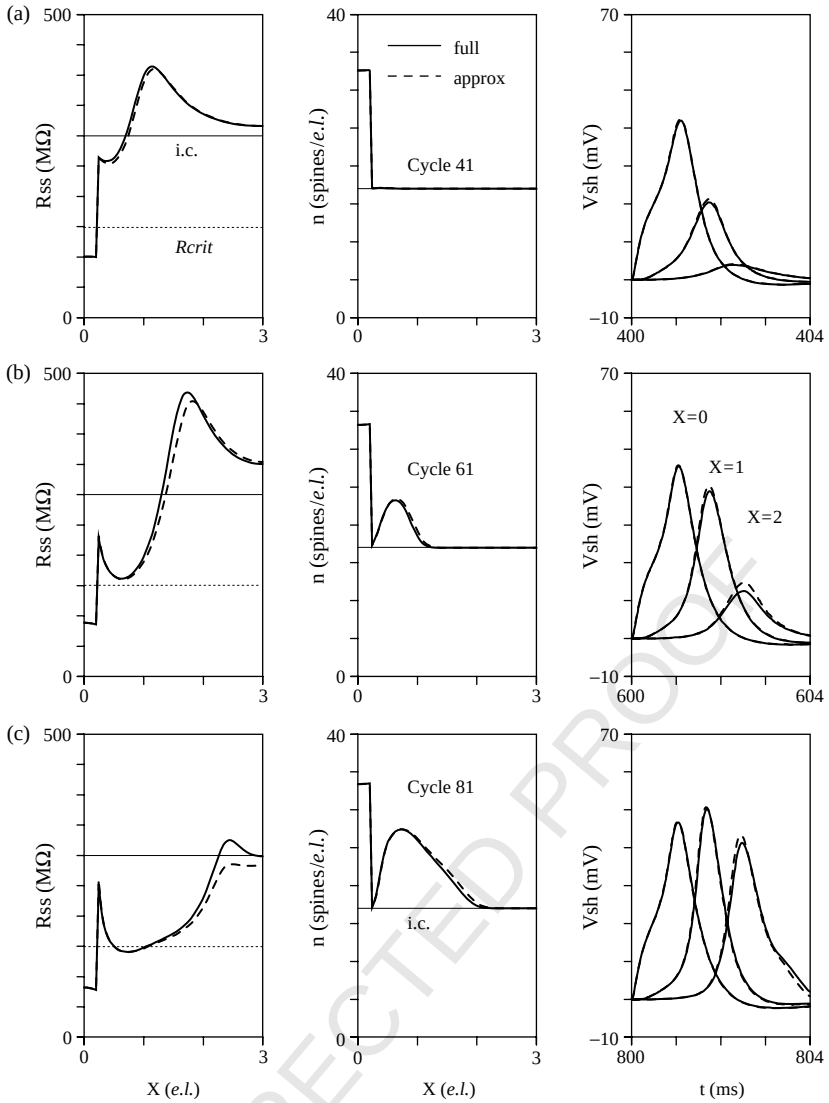

Figure 5. Approximating a mathematical description for activity-dependent synapse restructuring. A passive cable, with the same geometric and electrical parameters as in Fig. 4, has an initial uniform distribution of 54 excitable spines, only now the initial stem resistance is reduced to a uniform value of $R_{ss} = 300$ MΩ, above a lower value for $R_{\text{crit}} = 150$ MΩ. Spines are periodically activated as in Fig. 4 and results are superimposed for the full model (Section 2) and the reduced model (Section 3). The upper and lower bounds for stem resistance have been reduced to $R_{\text{max}} = 1000$ MΩ and $R_{\text{min}} = 40$ MΩ, respectively. (a) An a.p. generates after 40 cycles, when R_{ss} falls below R_{crit} and $\overline{n}$ almost doubles in the stimulated region. (b) The propagating wave causes a decrease in R_{ss} and a corresponding increase in $\overline{n}$ out to $X = 1.0$ after 60 activation cycles. The asymptotic error depends on the magnitude of R_{ss}. (c) The a.p. propagates to $X = 2.0$ as R_{ss} decreases and $\overline{n}$ increases behind the wave. In this structural configuration, the propagating wave reaches its greatest magnitude in the center of the dendrite [c.p. to Fig. 4(c)].

connected to the dendrite (shorter spine stems) in areas receiving a sustained high level of activity. Results also predict that areas of the dendrite experiencing a sustained lack of electrical activity (whether synaptic activation or current flowing along the dendrite) will have a higher percentage of spines with long, narrow stems. The length of time for structural transition depends on the magnitude of ϵ, selected here for computational efficiency. To achieve the results shown in this paper over 12–13 days, as observed by Geinisman *et al*. (1996), one would need to set the rate of change in spine structure on the order of $\epsilon = 10^{-7}$.

By allowing local spine density and structure to transition through identified threshold values for generation of a.p., new pathways are created for wave propagation when the spines are modeled with excitable membrane properties. Results shown here are for a dendrite of physical length 3λ, where λ is approximately 180 μm. This means that the signal propagation in Fig. 4(c) represents a wave of a.p.s extending to a physical length of $x = 0.36$ mm, resulting from synaptic activation (I_{syn}) of seven axodendritic synapses ($R_{ss} = 250$ MΩ) located between $x = 0.0$ and 0.036 mm, along with the evolving profile for spine density and structure from previous synaptic events.

The paper deals with the disparity of time scales between rapid changes in activity and slow changes in morphology. Comparative simulations identify a parameter value for the rate of change in the slow system that returns results in a shorter period of computation time, without sacrificing the dynamics of the system for smaller values of the parameter. Another way to speed up computation time in systems with periodic activation would be to exploit the fact that the slow variables are piecewise continuous over time and relatively constant within each activation cycle. One might then use the average measure of local activity in each cycle to compute changes in the slow system at the end of each cycle of length T, rather than integrating the entire system at each time step. For example, changes in spine structure over each cycle may alternately be derived as

$$\frac{R_{ss}(X, T_i) - R_{ss}(X, T_{i-1})}{T} = -\epsilon f(R_{ss}(X, T_{i-1})) \int_{T_{i-1}}^{T_i} I_{ss}(X, t)dt \qquad (14)$$

$$R_{ss}(X, T_i) = -T\epsilon f(R_{ss}(X, T_{i-1}))I_{ss}^{\text{avg}}(X) + R_{ss}(X, T_{i-1}), \qquad (15)$$

where the average stem current is computed as the total contribution I_{ss} over each cycle divided by the length of the cycle

$$I_{ss}^{\text{avg}} = \frac{1}{T} \int_{T_{i-1}}^{T_i} I_{ss}(X, t)dt. \qquad (16)$$

Calcium from internal stores was recently shown to cause elongation of dendritic spine stems in slice cultures (Korkortian and Segal, 1999). Still another

experiment indicates that increased calcium levels may cause spine stem shortening (Halpein *et al*., 1998). Harris (1999b) proposes yet another model for spine restructuring based upon the above experiments: A moderate amount of synaptic activation may cause calcium to be released from a cell's internal stores, resulting in spine stem elongation. However, a higher level of activity may cause calcium influx and induce spine stem shortening or loss (Harris, 1999b). Cable theory (Baer and Rinzel, 1991) allows for dynamic molecular elements in a continuum of spines, and one could begin to model calcium-dependent, bi-directional changes in spine structure using a slow subsystem to the cable model to capture these experimental observations.

ACKNOWLEDGEMENTS

This research was conducted with support from NSF DBI-9602226: Research Training Grant-Nonlinear Dynamics in Biology, awarded to the University of California, Davis; and faculty grant-in-aid Number 242122 from San Diego State University. The author gratefully acknowledges S. M. Baer of Arizona State University for helpful discussions, and Armando Solorzano of El Centro, CA for graphics.

APPENDIX A

A.1. Table of parameters.

A_{sh}	Surface area of each spine head	1.31 μm^2
β	Rate of change in stem resistance	30
C_m	Specific membrane capacitance	1 μFcm^2
C_{sh}	Capacitance of each spine head	$A_{sh}C_m$
d	Diameter of the dendrite	0.36 μm
δ	Perturbation parameter	R_{ss}/R_∞
ϵ	Rate of change in stem resistance	0.02
γ	Channel density	2.5
g_p	Peak synaptic conductance	0.074 nS
$\overline{\overline{g}}_K$	Maximal potassium conductance	36 mS cm^{-2}
$\overline{\overline{g}}_L$	Maximal leakage conductance	0.3 mS cm^{-2}
$\overline{\overline{g}}_{Na}$	Maximal sodium conductance	120 mS cm^{-2}
λ	Length constant	$\sqrt{R_m d/4R_i}$
R_{crit}	Critical value for stem resistance	300 MΩ (Section 2) 150 MΩ (Section 3)
R_i	Specific cytoplasmic resistivity	70 Ω cm
R_∞	Input resistance	$R_m/(\lambda\pi d)$
R_m	Passive membrane resistance	2500 Ω cm^2
R_{max}	Stem resistance upper bound	2000 MΩ (Section 2) 1000 MΩ (Section 3)
R_{min}	Stem resistance lower bound	200 MΩ (Section 2) 40 MΩ (Section 3)
R_{sh}	Resistance of each spine head	$1.02 \times 10^{11}\Omega$
τ_m	Membrane time constant	$R_m C_m$

t_p	Time to peak in each activation cycle	0.2 ms
V_K	Potassium reversal potential	−12 mV
V_L	Leakage reversal potential	10.5989 mV
V_{Na}	Sodium reversal potential	115 mV
V_{syn}	Synaptic reversal potential	100 mV

A.2. Activity-dependent synapse restructuring.

$$\tau_m \frac{\partial V_d}{\partial t} = \frac{\partial^2 V_d}{\partial X^2} - V_d + R_\infty \overline{n} I_{ss} \tag{A.1}$$

$$C_{sh} \frac{\partial V_{sh}}{\partial t} = -I_{\text{ion}} - I_{\text{syn}} - I_{ss} \tag{A.2}$$

$$\frac{\partial R_{ss}}{\partial t} = -\epsilon R_{ss}^2 I_{ss} \left(1 - \frac{R_{ss}}{R_{\max}}\right)\left(\frac{R_{ss}}{R_{\min}} - 1\right) \tag{A.3}$$

$$\overline{n}(X,t) = \overline{n}_0 \left[\frac{m+1}{2} - \frac{m-1}{2} \tanh \frac{\beta(R_{ss}(X,t) - R_{\text{crit}})}{R_\infty}\right], \tag{A.4}$$

where

$$I_{ss} = \frac{V_{sh} - V_d}{R_{ss}} \tag{A.5}$$

$$I_{\text{syn}} = g_p \frac{t}{t_p} e^{\left(1 - \frac{t}{t_p}\right)} (V_{sh} - V_{\text{syn}}). \tag{A.6}$$

Ionic current in the passive or excitable spines is modeled, respectively by

$$I_{\text{ion}} = V_{sh}/R_{sh} \tag{A.7}$$

or

$$I_{\text{ion}}(V_{sh}, X, t) = \gamma A_{sh}((V_{sh} - V_{Na})\overline{g}_{Na} m^3 h + (V_{sh} - V_K)\overline{g}_K n^4 + (V_{sh} - V_L)\overline{g}_L). \tag{A.8}$$

The boundary and initial conditions are, respectively,

$$\frac{\partial V_d}{\partial X}(0,t) = 0.0 \tag{A.9}$$

$$\frac{\partial V_d}{\partial X}(L,t) = 0.0. \tag{A.10}$$

and

$$V_{sh}(X,0) = V_d(X,0) = 0.0. \tag{A.11}$$

A.3. Reduced model for synapse restructuring.

$$(\tau_m + R_\infty \overline{n} C_{sh}) \frac{\partial V_d}{\partial t} = \frac{\partial^2 V_d}{\partial X^2} - V_d - \overline{n} R_\infty (I_{\text{ion}}(V_d) + I_{\text{syn}}(V_d)) \tag{A.12}$$

$$\frac{\partial R_{ss}}{\partial t} = -\epsilon R_{ss}^2 I_{ss} \left(1 - \frac{R_{ss}}{R_{\max}}\right) \left(\frac{R_{ss}}{R_{\min}} - 1\right) \tag{A.13}$$

$$\overline{n}(X,t) = \overline{n}_0 \left(\frac{m+1}{2} - \frac{m-1}{2} \tanh \frac{\beta(R_{ss}(X,t) - R_{\text{crit}})}{R_\infty}\right), \tag{A.14}$$

where

$$I_{ss} = \frac{W_0}{R_\infty} \tag{A.15}$$

$$W_0 = -R_\infty \left(C_{sh} \frac{\partial V_d}{\partial t} + I_{\text{ion}}(V_d) + I_{\text{syn}}(V_d)\right). \tag{A.16}$$

Synaptic and ionic currents (I_{syn} and I_{ion}), as well as initial and boundary conditions are as in the full model above. The reduced model introduces a first-order measure for local activity that may be used to approximate I_{ss} in other models when R_{ss} is small (Wu and Baer, 1998; Verzi and Baer, 2000).

A.4. Stability analysis for the cable equation. When R_{ss}/R_∞ is small, the electrical coupling between the spine and dendritic shaft is strong. Moreover, the governing equations (1)–(3) become singular. One can easily see this by substituting equation (3) into (1), namely

$$\tau_m \frac{\partial V_d}{\partial t} = \frac{\partial^2 V_d}{\partial X^2} - V_d + \frac{R_\infty}{R_{ss}} \overline{n} (V_{sh} - V_d). \tag{A.17}$$

Multiply through by $\delta = R_{ss}/R_\infty$ to obtain

$$\delta \tau_m \frac{\partial V_d}{\partial t} = \delta \frac{\partial^2 V_d}{\partial X^2} - \delta V_d + \overline{n} (V_{sh} - V_d). \tag{A.18}$$

For $\delta \ll 1$, both time and spatial derivatives have a small coefficient. In the limit, $\delta \to 0$ and the problem becomes singular.

REFERENCES

Baer, S. M. and J. Rinzel (1991). Propagation of dendritic spikes mediated by excitable spines: a continuum theory. *J. Neurophysiol.* **65**, 874–890.

Boyer, C., T. Schikorski and C. F. Stevens (1998). Comparison of hippocampal dendritic spines in culture and in brain. *J. Neurosci.* **18**, 5294–5300.

Coombes, S. and P. C. Bressloff (2000). Solitary waves in a model of dendritic cable with active spines. *SIAM J. Appl. Math.* **61**, 432–453.

Edwards, F. A. (1995). LTP–a structural model to explain the inconsistencies. *TINS* **18**, 250–255.

FitzHugh, R. (1969). Mathematical models for excitation and propagation in nerve, in *Biological Engineering*, H. P. Schwan (Ed.), New York: McGraw-Hill.

Geinisman, Y., L. Detoledo-Morrell, F. Morrell, R. E. Heller, M. Rossi and R. F. Parshall (1993). Structural synaptic correlate of long-term potentiation: formation of axospinous synapses with multiple, completely partitioned transmission zones. *Hippocampus* **3**, 435–446.

Geinisman, Y., L. deToledo-Morrell, F. Morrell, I. S. Persina and M. A. Beatty (1996). Synapse restructuring associated with the maintenance phase of hippocampal long-term potentiation. *J. Comp. Neurol.* **368**, 413–423.

Halpein, S., A. Hipolito and L. Saffer (1998). Regulation of F-actin stability in dendritic spines by glutamate receptors and calcineurin. *J. Neurosci.* **18**, 9835–9844.

Harris, K. M. (1999a). Structure, development, and plasticity of dendritic spines. *Curr. Opin. Neurobiol.* **9**, 343–348.

Harris, K. M. (1999b). Calcium from internal stores modifies dendritic spine shape. *Proc. Natl. Acad. Sci.* **96**, 12213–12215.

Hodgkin, A. and A. Huxley (1952). A quantitative description of membrane current and its application to conduction and excitation in nerve. *J. Physiol. (Lond.)* **117**, 500–544.

Korkortian, E. and M. Segal (1999). Release of calcium from stores alters the morphology of dendritic spines in cultured hippocampal neurons. *Proc. Natl. Acad. Sci.* **96**, 12068–12072.

Luscher, C., R. A. Nicoll, R. C. Malenka and D. Muller (2000). Synaptic plasticity and dynamic modulation of the post synaptic membrane. *Nat. Neurosci.* **3**, 545–550.

Maletic-Savatic, M., R. Malinow and K. Svoboda (1999). Rapid dendritic morphogenesis in CA1 hippocampal dendrites induced by synaptic activity. *Science* **283**, 1923–1927.

Poznanski, R. R. and J. Bell (2000). A dendritic cable model for the amplification of synaptic potentials by an ensemble average of persistent sodium channels. *Math. Biosci.* **166**, 101–121.

Rall, W. and J. Rinzel (1971). Dendritic spine function and synaptic attenuation calculations. *Prog. Abstr. Soc. Neurosci.* **1**, 64.

Segev, I. and W. Rall (1988). Computational study of an excitable dendritic spine. *J. Neurophysiol.* **60**, 499–523.

Segev, I. and W. Rall (1998). Excitable dendrites and spines: earlier theoretical insights elucidate recent direct observations. *Trends Neurosci.* **21**, 453–460.

Shepherd, G. M. (1996). The dendritic spine: a multifunctional integrative unit. *J. Neurophysiol.* **75**, 2197–2210.

Sorra, K. E., J. C. Fiala and K. M. Harris (1999). Critical assessment of the involvement of perforations, spinules, and spine branching in hippocampal synapse formation. *J. Comp. Neurol.* **398**, 225–240.

Svoboda, K. (1999). Optical studies of single synapses in brain slices. *Biophys. J.* **76**, A142 part 2.

Svoboda, K., D. W. Tank and W. Denk (1996). Direct measurement of coupling between dendritic spines and shafts. *Science* **272**, 716–719.

Tsay, D. and R. Yuste (2002). Role of dendritic spines in action potential back propagation: a numerical simulation study. *J. Neurophysiol.* **88**, 2834–2545.

Verzi, D. W. (2000). A mathematical description of diagrammatic models for activity-dependent spine structures, PhD thesis, Arizona State University.

Vetter, P., A. Roth and M. Hausser (2001). Propagation of action potentials in dendrites depends on dendritic morphology. *J. Neurophysiol.* **85**, 926–937.

Wu, H. Y. and S. M. Baer (1998). Analysis of an excitable dendritic spine with an activity-dependent stem conductance. *Bull. Math. Biol.* **36**, 569–592.

Received 3 March 2003 and accepted 20 October 2003